

# Perovskite B-Site Compositional Control of [110]<sub>p</sub> Polar Displacement Coupling in an Ambient-Pressure-Stable Bismuth-based Ferroelectric\*\*

Michelle R. Dolgos, Umut Adem, Alicia Manjon-Sanz, Xinming Wan, Tim P. Comyn, Timothy Stevenson, James Bennett, Andrew J. Bell, T. Thao Tran, P. Shiv Halasyamani, John B. Claridge,\* and Matthew J. Rosseinsky\*

Piezoelectrics are key functional materials in actuator and sensor applications.<sup>[1]</sup> Current technology exploits lead-based materials displaying a morphotropic phase boundary (MPB) between two ferroelectric solid solutions of different symmetries and polarization directions. This is best exemplified by the  $\text{PbZr}_{1-x}\text{Ti}_x\text{O}_3$  (PZT) perovskite system where the distortions driving the piezo response are produced by the stereo-active electron lone pair of the  $\text{Pb}^{2+}$  cation on the A site of the  $\text{ABO}_3$  perovskite structure.<sup>[2]</sup> Due to the environmental impact of lead, there is a considerable focus on the synthesis of lead-free electroceramics. It is not however clear if the complex crystal chemistry underlying the structural phase boundaries at the MPB in lead-based systems can be simply translated into lead-free analogues. In particular the balance between distortions driven by the A and B site cations and the role of octahedral tilting and tolerance factor considerations are expected to be quite different in non-lead systems, as  $\text{Pb}^{2+}$  is significantly larger than the more highly charged  $\text{Bi}^{3+}$  often considered as an alternative polarization-generating cation.<sup>[3]</sup> However, the smaller size of bismuth ions generally requires high-pressure synthesis conditions to form a perovskite. Only a small group of known perovskites exist with A-site bismuth cations that are stable at ambient

pressure, based on  $\text{BiFeO}_3$ ,<sup>[4]</sup>  $\text{Bi}_2\text{Mn}_{4/3}\text{Ni}_{2/3}\text{O}_6$ ,<sup>[5]</sup> and  $\text{Bi}(\text{Fe}_{2/8}\text{Ti}_{3/8}\text{Mg}_{3/8})\text{O}_3$  (BFTM).<sup>[6]</sup>  $\text{Bi}_2\text{Mn}_{4/3}\text{Ni}_{2/3}\text{O}_6$  is antiferrodisplacive,<sup>[5]</sup> while both  $\text{BiFeO}_3$  and BFTM adopt the  $R'$   $R3c$  structure where the  $[111]_p$  displacements of untilted R (space group  $R3m$  in the PZT case) are coupled with octahedral rotation about the same axis (the prime symbol denotes the presence of tilts). In order to access MPBs, polar structures with distinct polarization directions away from  $[111]_p$  in these Bi-based families are required.

We investigated the pseudoternary phase field BFTM– $\text{LaFeO}_3$  (LFO)– $\text{La}_2\text{MgTiO}_6$  (LMT) where the introduction of LFO (tolerance factor  $t=0.95$ ) would alter the average structural asymmetry on the A site by combining the aspherical  $\text{Bi}^{3+}$  and spherical  $\text{La}^{3+}$  cations, and the addition of  $\text{Mg}^{2+}$  and  $\text{Ti}^{4+}$  from LMT ( $t=0.95$ ) on the B site would reduce the dielectric loss caused by the increase in  $\text{Fe}^{3+}$  content. LFO adopts the  $Pmnb$  structure of  $\text{GdFeO}_3$  with an  $a^+b^-b^-$  tilt system and  $0.18 \text{ \AA}$  antiferrodistortive  $\text{La}^{3+}$  displacements along the  $[110]_p$  direction. LMT ( $P2_1/a$ ) has the same A-site displacement pattern and tilt system plus rock salt ordered B-site cations.<sup>[7]</sup>

Phases in the BFTM–LMT–LFO (BLFTM) field (Figure 1a) were prepared according to the protocol set out in Section 1 of the Supporting Information. Four distinct classes of powder diffraction patterns are observed. BFTM ( $t=0.96$ ) is the only material with the rhombohedral  $R3c$  space group, and is surrounded by a two-phase region. At low LFO content and along the BFTM–LMT line, an orthorhombic perovskite phase and an Aurivillius phase coexist (XRD data Figure S1, Supporting Information). However, single phases emerge at higher substitution levels. These phases adopt the nonpolar  $Pmnb$  structure at high LFO/LMT content, but a new orthorhombic phase emerges between the  $Pmnb$  and multiphase regions, as shown by the evolution of the lattice parameters along the  $(1-x)\text{BFTM}-x\text{LFO}$  line in Figure 1b. Powder second harmonic generation (SHG) measurements<sup>[8]</sup> show that the non- $Pmnb$  BLFTM samples are non-centric ( $x=0.28, 0.37, 0.40, 0.42$ ), whereas the  $Pmnb$  materials ( $x=0.5, 0.67$ ) are centric as expected. Thin films can be grown by pulsed laser deposition (Section 5, Supporting Information).

The structural characterization of the new non-centric BLFTM phase will focus on the  $\text{Bi}_{0.72}\text{La}_{0.28}(\text{Fe}_{0.46}\text{Ti}_{0.27}\text{Mg}_{0.27})\text{O}_3$  (0.72BFTM–0.28LFO) composition. Of the candidate space groups which gave similar model-independent Le Bail fits in the observed  $2a_p \times \sqrt{2}a_p \times \sqrt{2}a_p$  cell only  $Pmnb$  and  $Pmc2_1$  give acceptable Rietveld refine-

[\*] M. R. Dolgos, U. Adem, A. Manjon-Sanz, X. Wan, J. B. Claridge, M. J. Rosseinsky  
Department of Chemistry, University of Liverpool  
Liverpool, L69 7ZD (UK)  
E-mail: claridge@liv.ac.uk  
m.j.rosseinsky@liv.ac.uk

T. P. Comyn, T. Stevenson, J. Bennett, A. J. Bell  
Institute for Materials Research, University of Leeds  
Leeds, LS2 9JT (UK)

T. T. Tran, P. S. Halasyamani  
University of Houston, Department of Chemistry  
Houston, TX 77204 (USA)

[\*\*] This work is funded by the European Research Council (M.D. is supported by ERC Grant agreement 227987 RLUCIM), the EPSRC (U.A. is supported by EP/H000925) and the Northwest Development Agency through the Knowledge Centre for Materials Chemistry. A.M.S. is supported by the European Union by the SOPRANO project (Grant No. PITN-GA-2008-214040). We thank ESRF (ID31) and ISIS (HRPD, GEM) for diffraction instrument access, and Prof. A. Fitch (ESRF) and Dr. K. S. Knight (ISIS) for their input into this work. P.S.H. and T.T.T. thank the Welch Foundation (Grant E-1457) for support.

Supporting information for this article is available on the WWW under <http://dx.doi.org/10.1002/anie.201203884>.

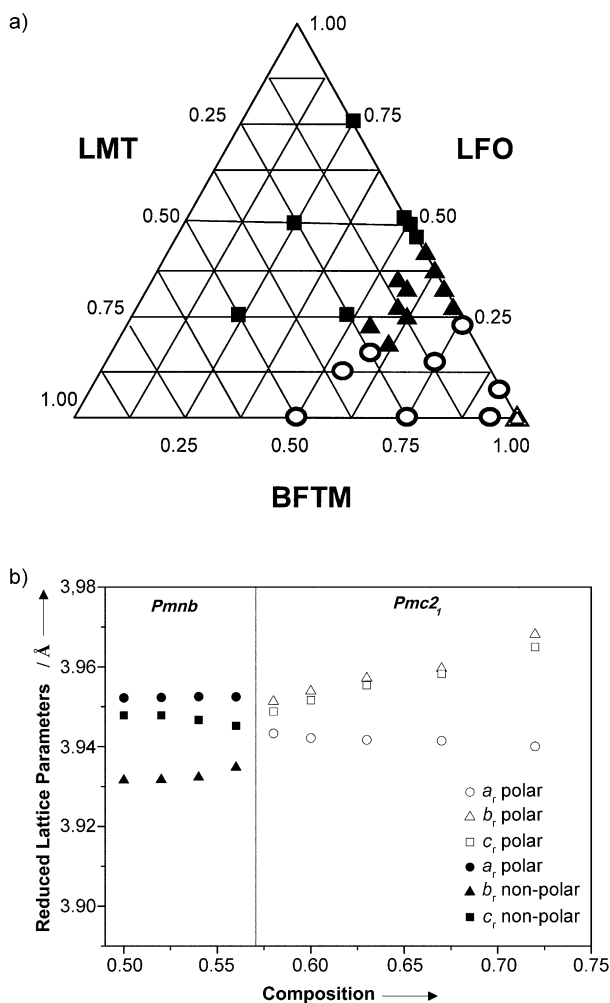


**Figure 1.** a) Phase diagram of the  $\text{Bi}(\text{Fe}_{2/8}\text{Ti}_{3/8}\text{Mg}_{3/8})\text{O}_3\text{-LaFeO}_3\text{-La}(\text{Mg}_{1/2}\text{Ti}_{1/2})\text{O}_3$  BLFTM system showing the four distinct categories of phase assemblage found in the system ( $\blacksquare$  *Pmnb*;  $\blacktriangle$  *Pmc2*<sub>1</sub>;  $\circ$  two-phase mixture;  $\triangle$  *R3c*) and b) evolution of the reduced lattice parameters along the BFTM–LFO line expressed as the composition of BFTM. Filled and open symbols correspond to materials shown to be centric and non-centric, respectively, by second harmonic generation measurements.

ments of neutron (HRPD, GEM) (Figure 2a) and synchrotron X-ray (ID31) data. The *Pmc2*<sub>1</sub> refinement is superior ( $R_{\text{wp}} = 7.19\%$  versus  $8.25\%$ ), with the non-polar *Pmnb* model unable to satisfactorily fit the (110), (200), and (011) reflections (Figure 2b).

The *Pmc2*<sub>1</sub> structure of 0.72BFTM–0.28LFO (Section 3.1, Supporting Information) is adopted at low temperature by the high-pressure form of the B-site-driven  $\text{CdTiO}_3$  ferroelectric,<sup>[9]</sup> (though more recent neutron diffraction studies have cast doubt on this<sup>[10]</sup>), the high field form of  $\text{NaNbO}_3$ <sup>[11]</sup> and sol-gel synthesized  $\text{NaNbO}_3$ .<sup>[12]</sup> There are one B site and two A sites in the asymmetric unit, with the Rietveld refinement showing no indication of Bi/La cation ordering. The two A sites are arranged in alternating layers along *a* (Figure 3a and b). Each A site has a ferroelectric displacement with a distinct amplitude ( $0.31 \text{ \AA}$  A1 and  $0.17 \text{ \AA}$  A2) along the *z* ( $[110]_p$ ) direction (Figure 3c), and distinct Bi–O environments (Fig-

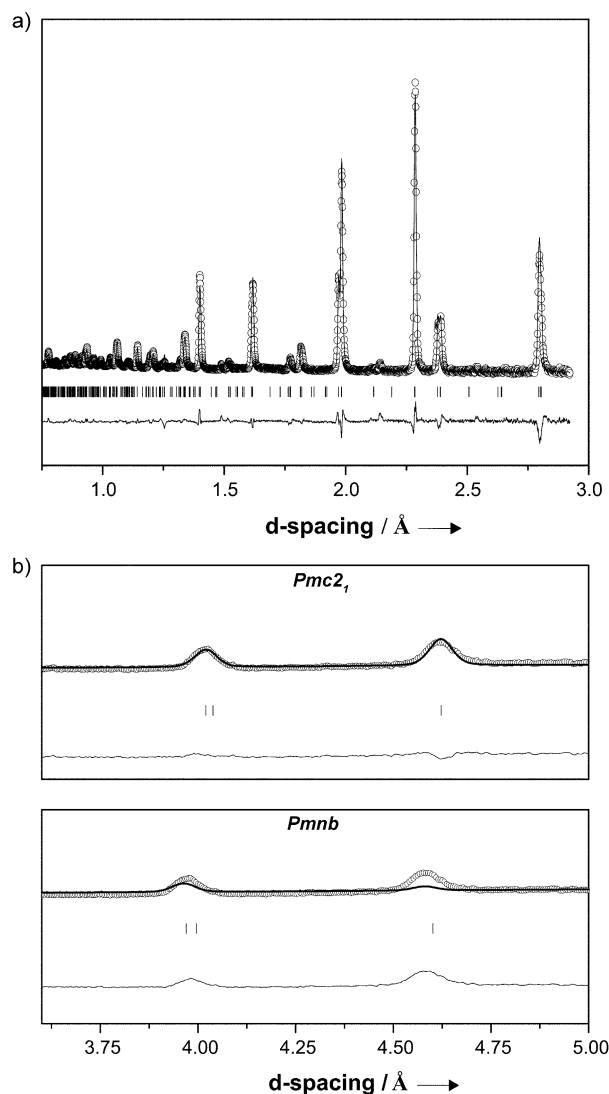


**Figure 2.** Rietveld refinement of a) neutron diffraction data (HRPD) for 0.72BFTM–0.28 LFO in space group *Pmc2*<sub>1</sub>. b) Comparison of the fits in *Pmc2*<sub>1</sub> (top) and *Pmnb* (bottom) for the (110), (200), and (011) reflections in 0.72BFTM–0.28LFO from the GEM neutron diffraction data. The circles represent the observed data, the thick line represents the model and the difference can be seen below.

ure 3 e,f). The B site (Figure 3g) also has a  $0.14 \text{ \AA}$  ferroelectric displacement along  $[110]_p$ . There are also small ( $< 0.05 \text{ \AA}$ ) antiferrodistortive displacements at both A sites along *b* and *c* and at the B site along *a* (Figure 3d). The ionic polarization calculated<sup>[13]</sup> from the refined structure is  $30.6 \mu\text{Ccm}^{-2}$ .

Measurement of the synchrotron X-ray and neutron powder diffraction patterns as a function of temperature reveals a structural phase transition from *Pmc2*<sub>1</sub> to *Pmnb* above  $650 \pm 5^\circ\text{C}$  (Figure S6). This structure (Section 3.2, Supporting Information) maintains the  $a^+b^-b^-$  tilt system of *Pmc2*<sub>1</sub>. There is only one crystallographically distinct A site, which is displaced  $0.08 \text{ \AA}$  antiferrodistortively along  $[110]_p$  and no B-site displacement.

The atomic displacements for the polar *Pmc2*<sub>1</sub> BLFTM structure and the high-temperature (HT) *Pmnb* phase can be understood in terms of distortion modes derived from the

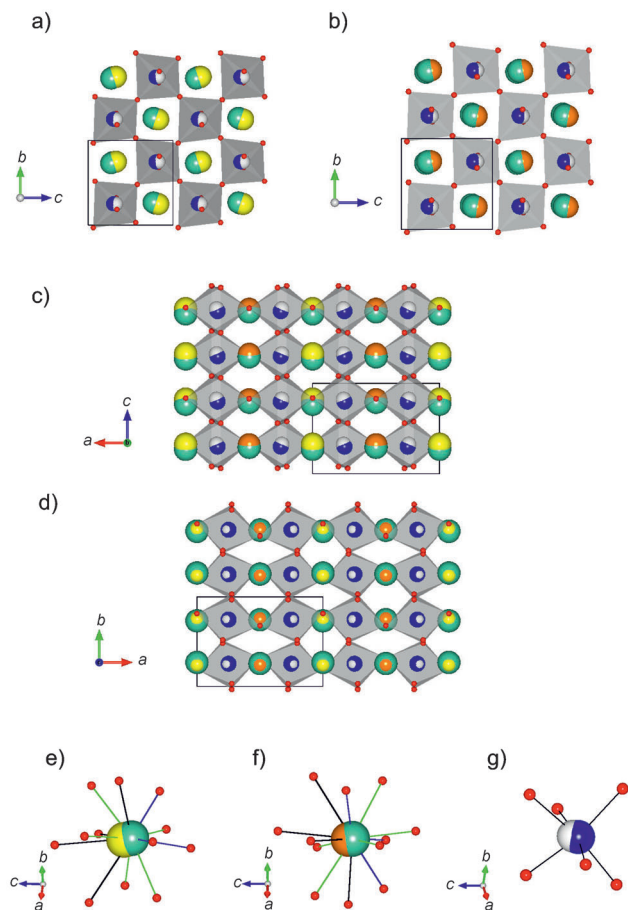


**Figure 3.**  $Pmc2_1$  room temperature structure of 0.72BFTM–0.28LFO. A-site cations represented in green, B-site cations blue, and oxygen atoms in red. The centroids of the oxide anions coordinating the A1 site are shown in yellow, A2 centroids orange, B centroids white. Viewed along the  $a$  direction, with a) the A1 layer on top and b) the A2 layer on top. c) Viewed along  $b$  showing the FE displacements of A1, A2, and B along the  $c$  direction. d) Viewed along  $c$  showing the A1 and A2 AFE displacements along  $b$  and the B-site AFE displacements along  $a$ . e) Coordination environment of the A1 cation. There are four short Bi–O contacts (blue) four intermediate (green) and four long bonds (black). Displacement components (0,  $-0.09$  Å,  $0.31$  Å) in the unit cell reference frame. f) Coordination environment of the A2 cation. This site has three short contacts (blue) and nine which are less distinctly separated than for A1, divided here into six bonds between 2.6 and 3 Å (green) and three bonds longer than 3 Å (black). Displacement components (0,  $-0.03$  Å,  $0.17$  Å). g) B-site octahedral environment. Displacement components: ( $-0.06$  Å,  $0.009$  Å,  $0.14$  Å).

$Pm\bar{3}m a_p$  aristotype cell, evaluated with the Isodisplace<sup>[14]</sup> and Amplimodes<sup>[15]</sup> programs (for further details and mode amplitudes see Section 3.3, Supporting Information).  $Pmnb$  (basis =  $\{(2,0,0), (0,1,-1)(0,1,1)\}$ , origin =  $(0,0,0)$ ) is produced by the  $R_4^+$  (Figure 4b) antiphase  $a^0b^-b^-$  and in-phase  $M_3^+$  (Figure S8a)  $a^+b^0b^0$  octahedral tilts which are the most significant modes. The associated antiferrodistortive A-site displacements along  $c$ ,  $0.08$  Å from the centroids of their coordinating oxygens, are from the  $X_5^+$  mode<sup>[16]</sup> (Figure 4c), giving the observed single A-site structure. The  $Pmc2_1$  phase (basis =  $\{(2,0,0), (0,1,-1)(0,1,1)\}$ , origin =  $(\frac{1}{2}, \frac{1}{2}, 0)$ ) is driven by the onset of the dominant  $\Gamma_4^-$  polar displacement at the A

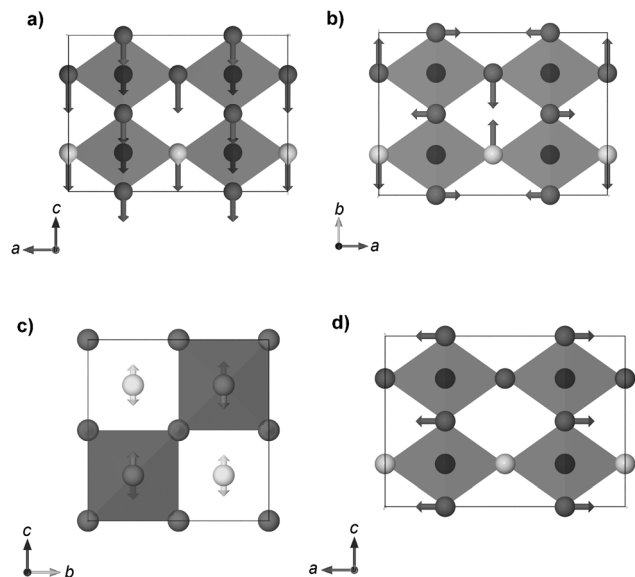


**Figure 4.** Important displacement modes in the  $Pmc2_1$  and  $Pmnb$  structures of BLFTM a)  $\Gamma_4^-$  ferroelectric displacement mode in  $Pmc2_1$ , b)  $R_4^+$  out-of-phase tilting mode (both structures), c) the  $X_5^+$  mode which is responsible for A-site antiferrodistortive displacements along  $c$  in both structures, and d) the  $X_3^-$  mode with antiferrodistortive B-site displacements along  $a$  in  $Pmc2_1$ . A-site cations represented in white, B-site cations black, and oxygen atoms in gray.

and B sites (Figure 4a). This ferroelectric displacement is along  $[110]_p$ , as in the  $Amm2$  (O) phase of  $BaTiO_3$ <sup>[17]</sup> and the high-field form of  $PbZrO_3$ .<sup>[18]</sup> In-phase combination of this ca.  $0.22$  Å magnitude polar displacement with the  $0.08$  Å antiferrodistortive displacement ( $X_5^+$  mode) present in the  $Pmnb$  precursor affords the  $0.31$  Å displacement at the A1 site, while the out-of-phase combination gives the  $0.14$  Å polar displacement at the A2 site along the  $[110]_p$  direction. The small A-site antiferrodisplacive  $R_5^+$  mode (Figure S8b) along  $b$  is unchanged between  $Pmnb$  and  $Pmc2_1$ . There is a single B site in  $Pmc2_1$  with the  $\Gamma_4^-$ -driven polar displacement along  $c$  accompanied by a smaller antiferroelectric displacement along  $a$  from the  $X_3^-$  mode (Figure 4d). Only one B site results because the ferroelectric and antiferroelectric displacement directions are perpendicular.

Electrical properties of BLFTM were measured on 97 + % dense ceramics, with dielectric loss reduced by the addition of 0.2 wt %  $MnO_2$ ,<sup>[19]</sup> which lowers  $\tan \delta$  from 0.036 to 0.025 at 1 kHz and from 0.589 to 0.034 at 1 Hz for 0.72BFTM–0.28 LFO. The low-frequency loss (Figure 5 a) is comparable to other shared A-site Bi-based ferroelectrics for example,  $Na_{0.5}Bi_{0.5}TiO_3$  ( $>0.05$  at 1 kHz).<sup>[20]</sup> 0.625BFTM–0.25LFO–0.125LMT has the lowest  $\tan \delta$ , suggesting that LMT is particularly effective in reducing the loss. All the  $Pmc2_1$   $[110]_p$  displaced materials have higher permittivities than  $[111]_p$  displaced rhombohedral BFTM, and the broad step-like decrease in permittivity for BFTM above 1 kHz, suggestive of a relaxation phenomenon, is not observed in the new polar phase. The magnitude of the relative permittivity rules out the possibility of contributions from extrinsic charge carriers at grain boundaries or electrode–sample interfaces.<sup>[21]</sup>

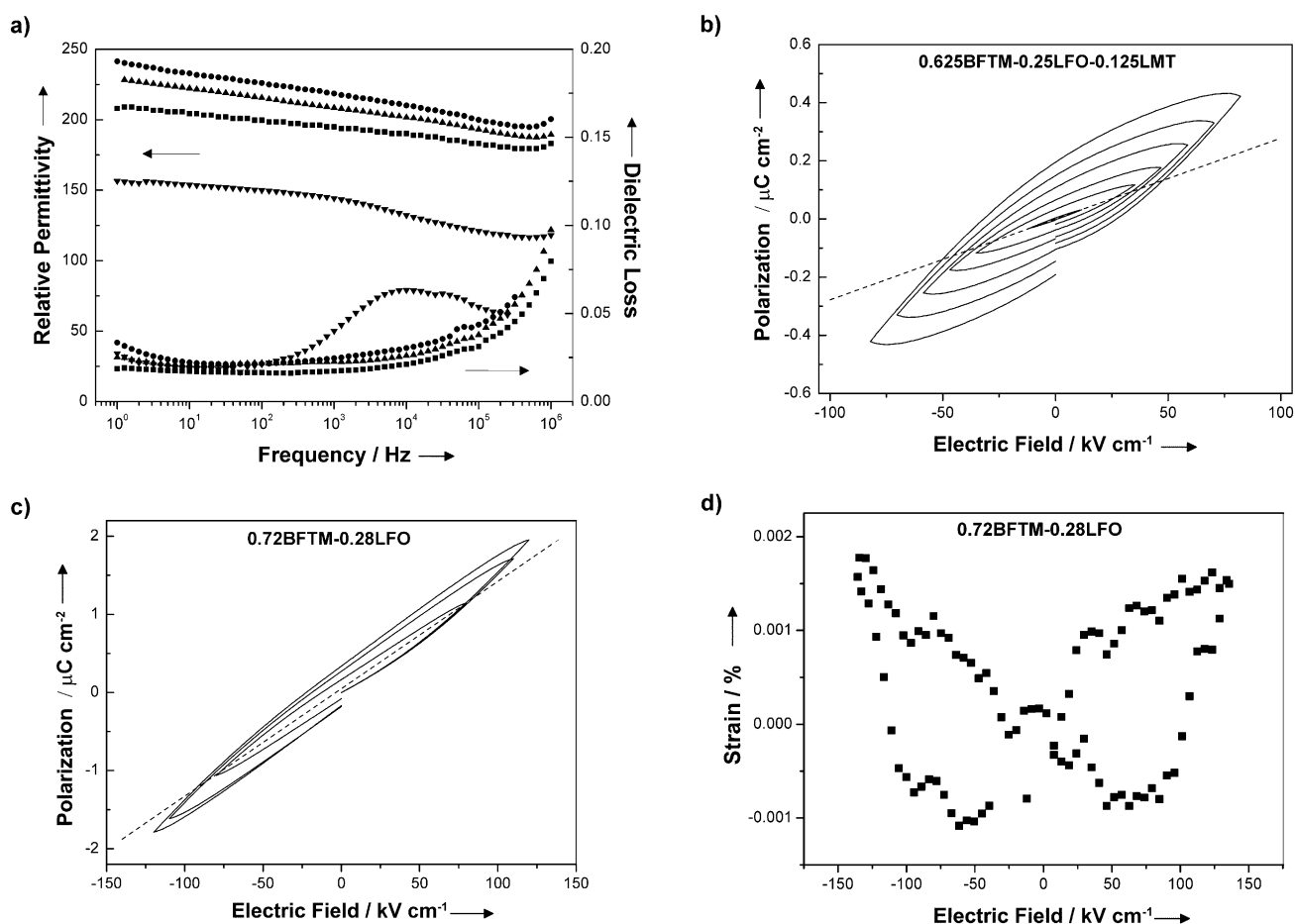


**Figure 5.** a) Room temperature permittivity and loss as a function of frequency of BFTM (▼), 0.72BFTM–0.28LFO (●), 0.625BFTM–0.25LFO–0.125LMT (■), and 0.58BFTM–0.42LFO (▲). b)  $P(E)$  loop for 0.625BFTM–0.25LFO–0.125LMT, c)  $P(E)$  loop for 0.72BFTM–0.28LFO corresponding to d) the strain-field loop of the same composition. The dotted line in (b) and (c) represent the slope of the  $P(E)$  loop at the lowest voltage and is used to demonstrate nonlinearity.

The polarity shown in the structure and SHG measurements was confirmed by measurements of piezoelectric behavior. Strain-field measurement on  $Pmc2_1$  0.72BFTM–0.28LFO (Figure 5d) shows a butterfly loop, with a negative strain component. This negative strain is related to domain back-switching during the bipolar cycles and demonstrates typical ferroelectric behavior.<sup>[22]</sup> The coercive field, calculated from the minimum in the strain field plot, is equal to  $62 \text{ kV cm}^{-1}$ . The calculated strain is 0.003 % and the high-field  $d_{33}$  value obtained from the strain-field measurements is  $1.68 \text{ pCN}^{-1}$ . The measured piezoelectric coefficient is  $0.25 \text{ pCN}^{-1}$ .

It was not possible to obtain a saturated  $P(E)$  ( $P$  = polarization,  $E$  = electric field) hysteresis loop before dielectric breakdown, which is a common problem in  $\text{BiFeO}_3$  ceramics.<sup>[23]</sup> This can be attributed to a high Curie temperature and coercive field. The best  $P(E)$  loop came from the  $Pmc2_1$  structure composition 0.625BFTM–0.25LFO–0.125LMT (Figure 5b). Although the loop is not saturated, electrical polarization does not evolve as a linear function of the driving-field amplitude indicating nonlinearity (a necessity for ferroelectrics) and therefore domain wall motion.<sup>[24]</sup>  $P(E)$  for 0.72BFTM–0.28LFO (Figure 5c) is not saturated but shows

non-linearity, indicating the presence of domain wall motion, consistent with the strain-field measurement on this composition.

Figure 6 represents the A-site displacements in polar structures derived from the ideal perovskite, with the effect of octahedral tilting in systems containing smaller A cations than  $\text{Pb}^{2+}$  evident. The  $O' Pmc2_1$  structure found here corresponds to the polarization direction changing from  $[111]_p$  in the  $R'$  parent phase BFTM to  $[110]_p$ , driven by the substitution of  $\text{La}^{3+}$  onto the A site, because of the tilts and displacements in this direction in  $\text{LaFeO}_3$ .  $\text{La}^{3+}$  substitution into  $R'$   $\text{BiFeO}_3$  also induces  $[110]_p$  A- and B-site displacements, but in this case the displacements are coupled *antiferrodistortively* to produce the antiferroelectric  $\text{PbZrO}_3$  structure (Figure 6;  $O_A'$  denotes a tilted antiferroelectric structure).<sup>[25]</sup> The striking difference in the coupling of the  $[110]_p$  displacements in the present BLFTM case may arise from the presence of  $\text{Mg}^{2+}$  and particularly  $\text{Ti}^{4+}$  on the B site in the BFTM parent, as  $\text{Ti}^{4+}$  produces ferroelectric  $[110]_p$  displacements in  $\text{O BaTiO}_3$ .<sup>[17]</sup> The  $O'$  structure features two A sites with distinct polarizations because of the competition between La-driven  $[110]_p$  antiferrodisplacive motions and the dominant ferroelectric displacements along the same direction driven by  $\text{Bi}^{3+}$  and

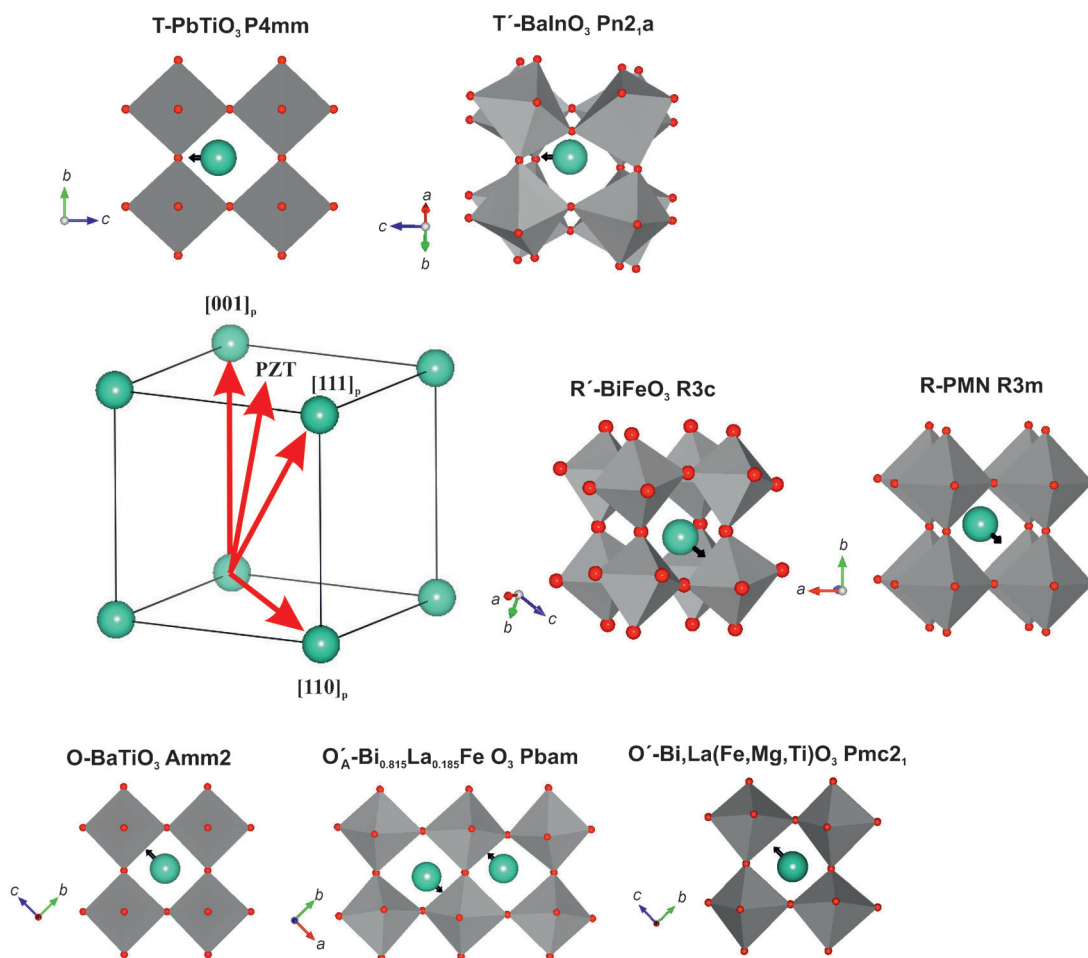


**Figure 6.** Examples of perovskites with A-site ferroelectric displacements along the  $[001]_p$ ,  $[110]_p$ , and  $[111]_p$  directions in relation to the ideal cubic perovskite  $a_p$  cell. The tilted  $T'$  structure of  $\text{BiInO}_3$  is only accessible at high pressure;<sup>[26]</sup> only the FE displacements are shown as the bismuth ion has an AFE component as well. The polar  $O'$  structure observed for BLFTM in the present study contrasts with the antiferrodistortive coupling of  $[110]_p$  displacements in the  $\text{PbZrO}_3$  structure of La-substituted  $R'$   $\text{BiFeO}_3$ . The arrow representing the displacements in M-PZT indicates a  $\text{Pb}^{2+}$  displacement mainly along  $[100]_p$ , but with a significant component along  $[110]_p$ .

$\text{Ti}^{4+}$ , reflecting structural frustration between the bonding preferences of the two A-site cations. In the present BLFTM system, the  $O'$  structure is separated by two-phase regions involving non-perovskite impurities from the  $R'$  structure, and bridging this phase gap is important in the search for enhanced functionality associated with potential phase boundaries differing in polarization direction.

Received: May 20, 2012

Published online: September 28, 2012

**Keywords:** bismuth · diffraction techniques · ferroelectricity · perovskites · polar structures

- [1] Y. Saito, H. Takai, T. Tani, T. Nonoyama, K. Takatori, T. Homma, T. Nagaya, M. Nakamura, *Nature* **2004**, 432, 84.  
 [2] a) T. Yamamoto, *Jpn. J. Appl. Phys.* **1996**, 35, 5104; b) R. Guo, L. E. Cross, S. E. Park, B. Noheda, D. E. Cox, G. Shirane, *Phys. Rev. Lett.* **2000**, 84, 5423.  
 [3] J. Rödel, W. Jo, K. T. P. Seifert, E.-M. Anton, T. Granzow, D. Damjanovic, *J. Am. Ceram. Soc.* **2009**, 92, 1153.

- [4] G. Catalan, J. Scott, *Adv. Mater.* **2009**, 21, 2463.  
 [5] H. Hughes, M. Allix, C. A. Bridges, J. B. Claridge, X. Kuang, H. Niu, S. Taylor, W. Song, M. J. Rosseinsky, *J. Am. Chem. Soc.* **2005**, 127, 13790.  
 [6] C. A. Bridges, M. Allix, M. R. Suchomel, X. Kuang, I. Sterianou, D. C. Sinclair, M. J. Rosseinsky, *Angew. Chem.* **2007**, 119, 8941; *Angew. Chem. Int. Ed.* **2007**, 46, 8785.  
 [7] a) A. N. Salak, O. Prokhnenko, V. M. Ferreira, *J. Phys. Condens. Matter* **2008**, 20, 085210; b) D.-Y. Lee, S.-J. Yoon, J. H. Yeo, S. Nahm, J. H. Paik, K.-C. Whang, B.-G. Ahn, *J. Mater. Sci. Lett.* **2000**, 19, 131.  
 [8] K. M. Ok, E. O. Chi, P. S. Halasyamani, *Chem. Soc. Rev.* **2006**, 35, 710.  
 [9] Y. J. Shan, H. Mori, K. Tezuka, H. Imoto, M. Itoh, *Ferroelectrics* **2003**, 284, 107.  
 [10] B. J. Kennedy, Q. Zhou, M. Avdeev, *J. Solid State Chem.* **2011**, 184, 2987.  
 [11] V. A. Shuvaeva, M. Y. Antipin, S. V. Lindeman, O. E. Fesenko, V. G. Smotrakov, Y. T. Struchkova, *Ferroelectrics* **1993**, 141, 307.  
 [12] K. E. Johnston, C. C. Tang, J. E. Parker, K. S. Knight, P. Lightfoot, S. E. Ashbrook, *J. Am. Chem. Soc.* **2010**, 132, 8732.  
 [13] S. C. Abrahams, *Acta Crystallogr. Sect. B* **2002**, 58, 34.  
 [14] B. J. Campbell, H. T. Stokes, D. E. Tanner, D. M. Hatch, *J. Appl. Crystallogr.* **2006**, 39, 607.

- [15] a) D. Orobengoa, C. Capillas, M. I. Aroyo, J. M. Perez-Mato, *Appl. Crystallogr.* **2009**, *42*, 820; b) J. M. Perez-Mato, D. Orobengoa, M. I. Aroyo, *Acta Crystallogr. Sect. A* **2010**, *66*, 820.
- [16] R. B. Macquart, B. J. Kennedy, M. Avdeev, *J. Solid State Chem.* **2010**, *183*, 2400.
- [17] G. Shirane, H. Danner, R. Pepinsky, *Phys. Rev.* **1957**, *105*, 856.
- [18] B. A. Scott, G. Burns, *J. Am. Ceram. Soc.* **1972**, *55*, 331.
- [19] S. O. Leontsev, R. E. Eitel, *J. Am. Ceram. Soc.* **2009**, *92*, 2957.
- [20] T. Wada, K. Toyoiike, Y. Imanaka, Y. Matsuo, *Jpn. J. Appl. Phys.* **2001**, *40*, 5703.
- [21] V. Bobnar, A. Levstik, C. Huang, Q. M. Zhang, *Phys. Rev. B* **2005**, *71*, 041202.
- [22] a) C. W. Ullah, A. Ahn, A. Hussain, S. Y. Lee, W. Kim, *J. Am. Ceram. Soc.* **2011**, *94*, 3915; b) T. P. Comyn, T. Chakraborty, R. E. Miles, S. J. Milne, *Appl. Phys. Lett.* **2008**, *93*, 052909.
- [23] a) W.-M. Zhu, H.-Y. Guo, Z.-G. Yea, *J. Mater. Res.* **2007**, *22*, 21362143; b) J. Wei, R. Haumont, R. Jarrier, Berhtet, Dkhil, *Appl. Phys. Lett.* **2010**, *96*, 102509.
- [24] S. Li, W. Cao, L. Cross, *J. Appl. Phys.* **1991**, *69*, 7219.
- [25] a) S. Karimi, I. M. Reaney, Y. Han, J. Pokorny, I. Sterianou, *J. Mater. Sci.* **2009**, *44*, 5102; b) I. Levin, S. Karimi, V. Provenzano, C. L. Dennis, H. Wu, T. P. Comyn, T. J. Stevenson, R. I. Smith, I. M. Reaney, *Phys. Rev. B* **2010**, *81*, 020103; c) D. A. Rusakov, A. M. Abakumov, K. Yamaura, A. A. Belik, G. Van Tendeloo, K. Takayama-Muromachi, *Chem. Mater.* **2011**, *23*, 285.
- [26] A. A. Belik, S. Y. Stefanovich, B. I. Lazoryak, E. Takayama-Muromachi, *Chem. Mater.* **2006**, *18*, 1964.